City Research Online

City, University of London Institutional Repository

This is the accepted version of the paper.

This version of the publication may differ from the final published version.

Design and Implementation of Spanwise Lift and Gust Control via Arrays of Bio-inspired Individually Actuated Pneumatic Flaplets

Alecsandra Court, Omar Selim, Keith Pamment and Christoph Bruecker

Department of Engineering, City, University of London, UK

ABSTRACT

Purpose
Covert feathers on avian wings can show dynamic pop-up behaviour in rapid succession as a reaction to turbulent gusts. The focus of the work is to understand the possible flow control mechanism induced during such dynamic motion cycles. A model aerofoil is designed with suction side spanwise control of rows of bio-inspired flaplets.

Approach
A NACA0012 aerofoil is equipped with a spanwise row of 8 flaplets at 80% chord, connected to pneumatic actuators and can be deployed to max 15° in a prescribed open-hold-close manner. The model is placed in a water-tunnel and flow measurements are done in the wake of the flaps during a cycle using Particle-Image-Velocimetry.

Findings
During opening, boundary layer flow is sucked into the void space between the wing surface and the flaplet, which induces backflow underneath the flaplet and traps the fluid inside. This fluid is expelled downstream during closure, which generates a forward directed jet as seen by the formation of a vortex-ring like structure with higher axial momentum. The entrainment of the jet leads to the re-energising of the boundary layer flow further upstream.

Originality
The paper presents a furtherment of understanding of the action of pop-up feathers for separation control. The actuation of the bio-inspired flaplets shows a flow vectorising effect which can be used for active separation and gust control. In the case of incipient separation, flaplet action can act to reattach the flow due to the jet entrainment effect.

1. INTRODUCTION

As technology advances, engineering and aviation seek ways to ever improve design, whether it be to better efficiencies or to discover new concepts of control mechanisms. The natural world has long since been looked at as an idea source and now, biomimicry models engineering design and production on the inspiration of natural processes. A system based on the ability that birds possess, allowing them to actively pop-up wing feathers during flight to change their aerodynamic parameters (Worcester, S. E, 1996), has been developed at City, University of London (Court, 2021) and will be the basis of this work. Biomimicry work has been carried out at City previously, investigating the dive pattern of a Peregrine Falcon (Selim, et al., 2021) and the flight control due to wing morphing, using wind tunnel tests and high fidelity simulations on idealised models. Owl-inspired passive trailing edge flaplets have also been investigated at City (Talboys, et al., 2019) for aerodynamic and aeroacoustic benefits. Such trailing edge flaplets have shown their benefit already as passive pace-makers to control non-linear instabilities in the boundary layer. Flying animals of various scales exploit sensors inherent within the stiffness of their feathers, for simultaneous flow sensing and control (Mohamed, A. et al, 2014). The current study uses a pneumatically actuated model, containing individual flaplets on the suction side of an aerofoil, to mimic the action of a pop-up feather.Such motion patterns can generate sucessive suction and vectorised blowing into the wake, which might be of benefit to prevent incipient stall or to counteract gust-induced flow separation.

The current concept is not comparable to a morphing wing with smooth trailing edge, as it is using flaplets on a rigid body aerofoil. It can be seen as an intermediate step for fixed wing structures to achieve improved control functionality. Fully flexible structures were investigated in (Pankonien & Inman, 2014), where complex spanwise camber variation was achieved without gaps and discontinuities. Another project that showed the benefits of a fully morphable wing was (Chanzy & Keane, 2018), in which twist morphing wings

were found to be more energy efficient during roll control.

The paper states, discusses and explains the design process and the initial testing of a finite wing section with 8 pneumatically actuated flaplets, on the suction side of a NACA0012 aerofoil. The pneumatic control permits fast response time of the flaplets, whilst the independently controllable flaplets allow for spanwise flow variation. The effective performance of the spanwise flaplets is analysed via particle image velocimetry (PIV) of the downstream wake section. The main objective of the project is to produce controllable and repeatable flaplet action and study the responsive flow pattern in a flow tunnel (water channel) to gain further knowledge of the interaction of the flow along the aerofoil and in the wake.

2. DESIGN AND CONSTRUCTION OF SPANWISE CONTROL CONCEPT

The control concept was originally developed from the finite spanwise lift control concept described in (Court, 2021). The design sought to adapt the circulation distribution along the span, using individually controllable pneumatically actuated flaps. The resultant model is currently being researched for studying the flow in a situation where the flaplets mimic the motion of the pop-up feathers. Therefore it is required to produce fast response, repeatable and consistent motion cycles of the flaplets, which can be controlled along the span individually to generate collective flaplet motion patterns along the array at different spanwise wavelengths (by setting the number of neighbouring actuators to run in simultaneous action.

The use of a pneumatic system was inspired by work such as (Siefert, et al., 2019), wherein mesostructured elastomer plates underwent fast, controllable, and complex shape transformations, at the input of pressure. The use of pneumatics in this project can allow for full baromorphing structures in future work, utilising the same pneumatic system. For this project it was chosen to use inflatable air cushions as actuators, which control the deployment motion of the flaplets. For ease of use, we applied latex balloon catheters (Latex Nelaton Ballonkatheter, Balloon volume 5-10ml Praxisdienst GmbH & Co KG, Germany) as they were a 'readymade' solution to the problem. During the flaplet deployment, an elastic rubber band is stretched inside the cavity, which ensures the return of the flaps towards the original

position flush with the aerofoil when pressures are reduced again to ambient. This ensures a quick return towards the original position.

The flaplets to be tested were hinged on a NACA0012 aerofoil of chord length 30cm and a finite span of 40cm. The trailing edge flaplet sections each had a span of 1.6cm and began at 80% chord length from the leading edge. The model utilised 3D printed sections to allow for ease of manufacture, assembly and repairability. All the trailing edge pieces slotted into the front portion of the aerofoil and can be removed individually.
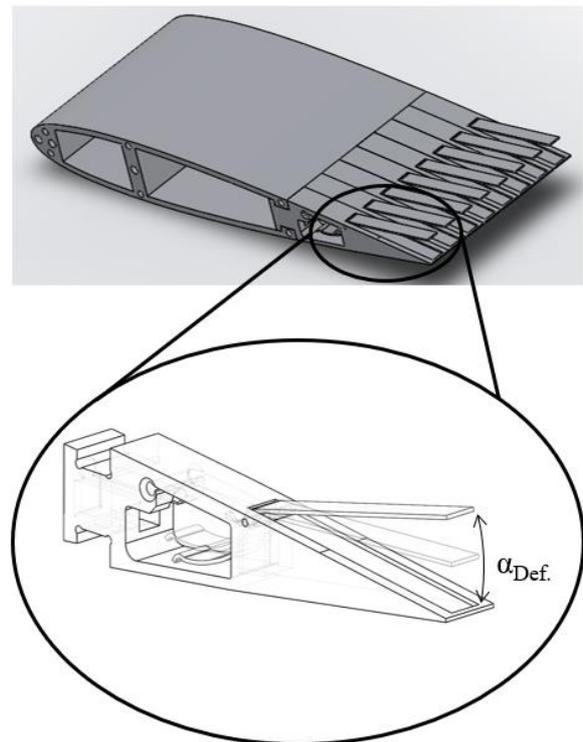

Figure 1: SolidWorks mock-up of the flaplet opening mechanism.
Source: This is an original figure produced by the authors.

Above in Fig. 1, is the SolidWorks model of the wing with one flaplet and its mechanism exaggerated. It should be noted that thin Perspex sheets were glued to each flaplet to ensure that the edge of each flaplet touched the edge of its neighbours, allowing no discontinuities. The physical realisation with a balloon is given in Fig. 2.

Figure 2: A single segment of the aerofoil with the balloon inside. Top: inflated situation with the flaplet deployed. Bottom: deflated position as the reference situation with the flaplet flush with the trailing edge. Source: This is an original figure produced by the authors.

The control of the pneumatic system is shown in below in Fig. 3, as a schematic diagram. The pneumatic valve system referenced was developed in a previous joint DFG project together with the IME, RWTH Aachen. It was used herein alongside an Arduino board to control the opening and closing of the individual valves in the valve block, and therefore individual flaplets. The regulator, valve block and pressure pipes used were also from Festo.
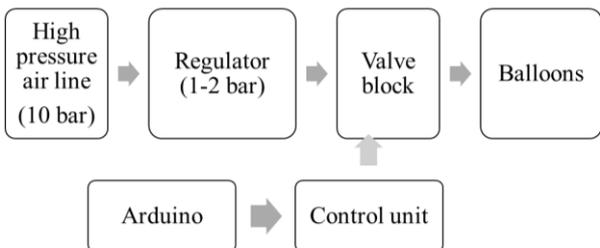

Figure 3: Schematic diagram of the pressure system. Source: This is an original figure produced by the authors.

3. WATER TUNNEL TEST

3.1 Experimental Setup

The model, as described in S*ection 2*, was tested in the water tunnel at City, University of London. A constant flow speed of $U_\infty = 5$cm/s was used, corresponding to a chord Reynolds-number of $Re_C = 15 \times 10^3$. The flow was suitably seeded with silver-coated ceramic particles of diameter 80µm (Hart Materials Limited, Tamworth,

UK), used as tracer particles. The goal was to capture clear TR-PIV results of the immediate flaplet and downstream wake and to study the flow dynamics of the flaplets actuating. A 3mm LED light sheet (IL-105/6X Illuminator, HardSoft, Germany) was used to illuminate the flow around the 5th flaplet in the horizontal plane.

The recordings of the flow were taken with a high-speed camera (Phantom Micro M310) mounted underneath the tunnel, pointed towards the LED light sheet via a mirror mounted at 45° (recordings at frame rates of 300fps, format 1280x800 px^2). Recordings were taken with different focal lengths, a larger field of view with 8x12 cm^2 was taken with a 100mm focal length and a zoomed in view with 4.5x6 cm^2, using a variable focal lens.

As displayed in Fig. 4, the model was mounted at AoA = 0˚ in the centre of the tunnel in all axes, for initial testing. For later testing, the model was mounted at a lifting angle of attack.
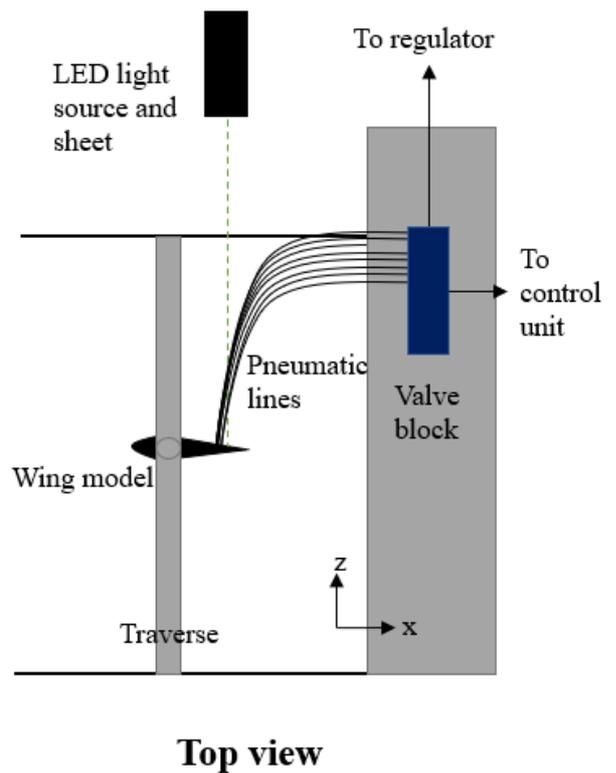

Top view

Figure 4a: Schematic of the experimental setup in the water tunnel, top view. Flow is in positive x-direction from left to right. Source: This is an original figure produced by the authors.
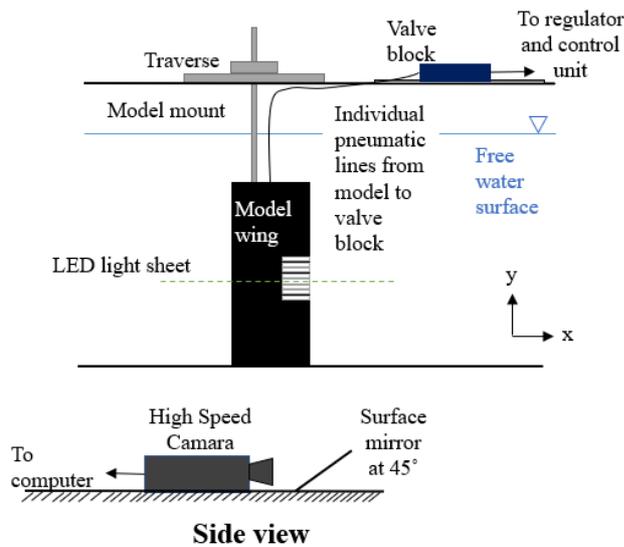
Figure 4b: Schematic of the experimental setup in the water tunnel, side view. Flow is in positive x-direction from left to right.
Source: This is an original figure produced by the authors.

3.2 Actuation Control

The flaplets were individually controllable via an Arduino board and Arduino IDE software connected to the valve control unit, see Fig. 3 The Arduino code outputted the instructions to the control unit and then therefore the valve block, regarding the pattern and opening or closing of each valve (total number of 20 valves). The valve block had high pressure air supplied via a regulator from a 10 bar pressure line input (regulated down to absolute pressure of 1.5 bar to stop the balloons from bursting). The opening of a valve allowed a specified balloon to inflate, and the closing allowed for ambient pressure to return and the balloon to deflate. The typical opening time of a balloon, after the pressure valve is opened, is about 200ms, similar to the closing time by the recoil action of the rubber band. To avoid bursting the balloons during extended phases of high pressure, a high frequency oscillatory pattern of pressure valve opening/closing is applied, which keeps the flaplets in their fully opened configuration with only marginal tip motion. Fig. 5 illustrates the state of 5 flaps deployed to full opening at the same time.

3.3 Test Description

The Arduino board was programmed to run the flaplet patterns and duty cycles. The first tested pattern was all flaplets up (flaplets 1-8), hold for 1s and then down again, whilst capturing live images. Testing of just one flaplet and then 8 flaplets with the model at an angle of attack were also carried out.
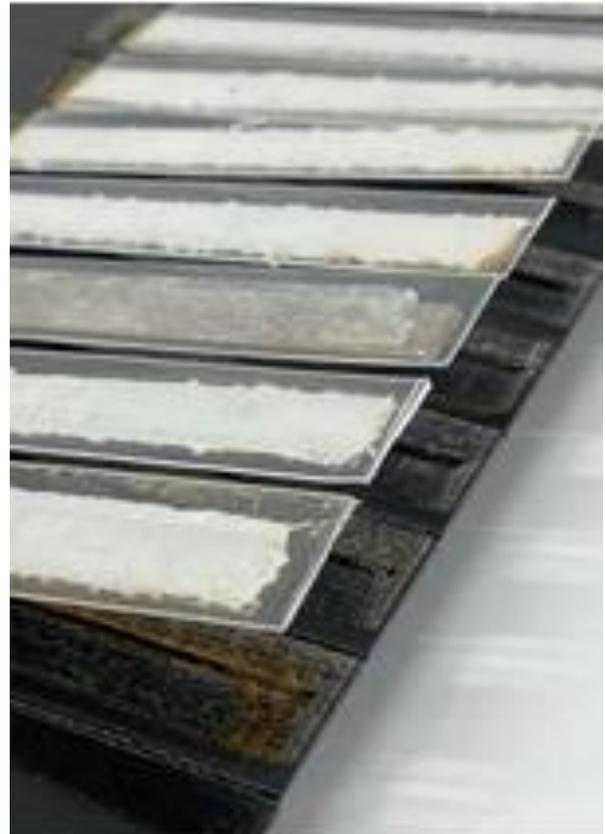

Figure 5: Flaplet actuation pattern used in the tests. All open.
Source: This is an original figure produced by the authors.

A picture of the complete setup with the LED light illuminating the plane of the 5th flaplet is shown below in Fig. 6, illustrating the overall arrangement of the measurement equipment together with the control unit on top of the tunnel.
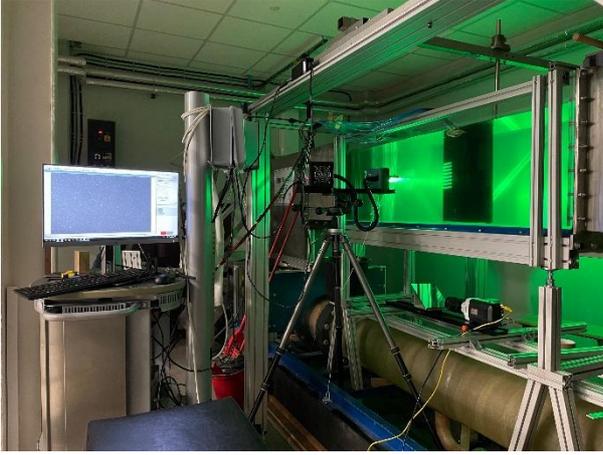
Figure 6: Picture of the water tunnel with the model inside and the optical setup for PIV measurements with LED light from the left and camera looking from the bottom.
Source: This is an original figure produced by the authors.

4. RESULTS

4.1 Zero lift condition

The idealised duty cycle generated within a flap opening and closing cycle is given in Fig. 7. It is adjusted in such a way, that the opening and closing velocities of the tip of the flaps reach values in the same order as the free-stream velocity.
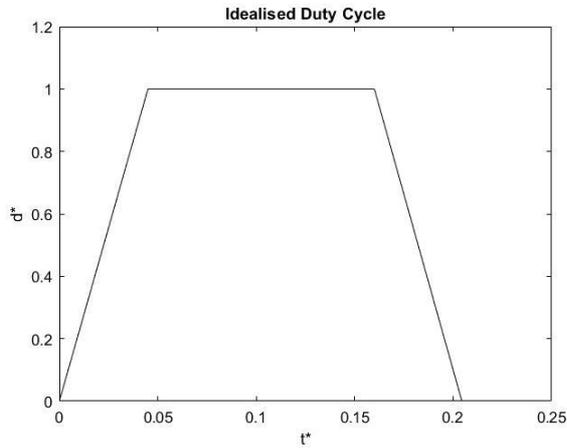

Figure 7: The idealised flaplet duty cycle, plotted.in non dimensionalised variables.
Source: This is an original figure produced by the authors.

Non dimensional distance, d* was plotted against non dimensional time t* in Fig. 7, where:

$$d^* = \frac{h(t)}{h(t_0)} \qquad Eq.\,(1)$$

$$t^* = \frac{tU_\infty}{C} \qquad Eq.\,(2)$$

Herein d* is in the range from full open (1) or closed (0). The deployment angle α_{Def} as shown in Fig. 1 has maximum value of α_{Max} 15˚, h is the wall-normal distance between the flaplet and the aerofoil model. The time t is in seconds and made dimensionless with the free stream velocity U_∞ (0.05m/s) and the chord C of the model (0.3m). The diagram shows the three phases within one actuation cycle, opening, hold and closing phase. At its fastest, by eliminating the hold phase of 0.15 convection times, the duty cycle can be completed in 0.1 convection times. A further evaluation of the induced exit velocity is discussed in the paragraph below and shown in Fig. 8. This is to introduce the idea of a squeezing effect which generates a tip exit velocity in streamwise direction near to the end of the closure phase.

Initial tests of the wake pattern for the actuation of all flaplets simultaneously, are shown by flow visualisation pictures in Fig. 9 during the cycle of a single sequence of opening and closing of the flaplets, as well as the reference flow. Those pictures are generated from the recorded image sequences, taken for TR-PIV. The light sheet is positioned along the mid-section of the 5th flaplet in the horizontal plane.

During the flaplet opening, a starting vortex is generated at the tip of the flaplet, while suction flow goes inwards into the void between the flaplet and the trailing edge. During the flaplet closure, this fluid portion is expelled in form of a jet back into the wake. The strong streamwise momentum of the jet causes acceleration of the flow at the trailing edge, into the former wake region, which is pushed further downstream. The entrainment of the jet leads to further flow acceleration at both sides of the trailing edge, which lasts until the formation of the wake begins again. Overall, this control cycle captures part of the wake fluid during flaplet opening and re-energises this fluid with the flaplet action during closure, interrupting the wake at the trailing edge with strong streamwise momentum. The current principle induces the momentum due to the squeezing effect, while the suction process entrains only fluid of low momentum from the near wake. The net effect is therefore argued to be helpful such as jet blowing, e.g., if local separation is happening.

The added streamwise momentum is apparent in Fig. 10a, as the velocity vectors are longer in the wake than they

are in the freestream post actuation of the flaplet. The added momentum was also quantified, as shown below, by considering the volume encapsulated by the open flaplet as a 3 dimensional wedge that decreases with decreasing deflection angle and time. By considering the mass flow rate, it can be said that the exit velocity as the flaplet closes, U_{exit}, is equivalent to the Eq. 3, below, where V is the volume of the wedge, A_{exit} is the exit area.

$$U(t)_{exit} = \frac{V(t)}{A(t)_{exit} t} \qquad Eq.(3)$$

The volume of the wedge is shown below, where b is the span of the flaplet (b=1.4cm), and L is the length of the flaplet (L=6cm).

$$V(t) = \frac{bh(t)L\cos(\alpha_{Def})}{2} \qquad Eq.(4)$$

The exit area is the decreasing rectangular area between the tip of the flaplet and the model.

$$A(t)_{exit} = bh(t) \qquad Eq.(5)$$

Substituting Eq. 4 and Eq. 5 into Eq.3 and considering time steps, the exit velocity can be calculated.

$$U(t_2)_{exit} = \frac{L[h(t_1)\cos(\alpha(t_1)) - h(t_2)\cos(\alpha(t_2))]}{h(t_2)(t_1 - t_2)} \qquad Eq.(6)$$

Fig. 8 below, is the non dimensionalised plot of Eq. (6). It can be seen that the exit velocity tends to infinity as deflection angle tends to zero. Which explains the increase in axial velocity seen in the results. This is due to the mechanism of converting the angular momentum of the flaplet retraction to axial momentum in the flow. This exit mechanism is similar to that shown in (Hess, et al., 2013).
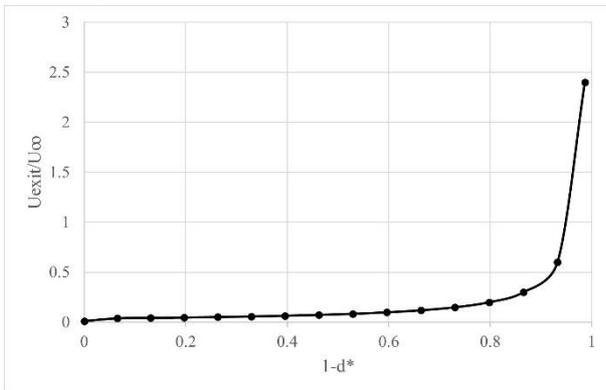

Figure 8: Tip exit velocity in streamwise direction against flaplet deflection angle during closure cycle.
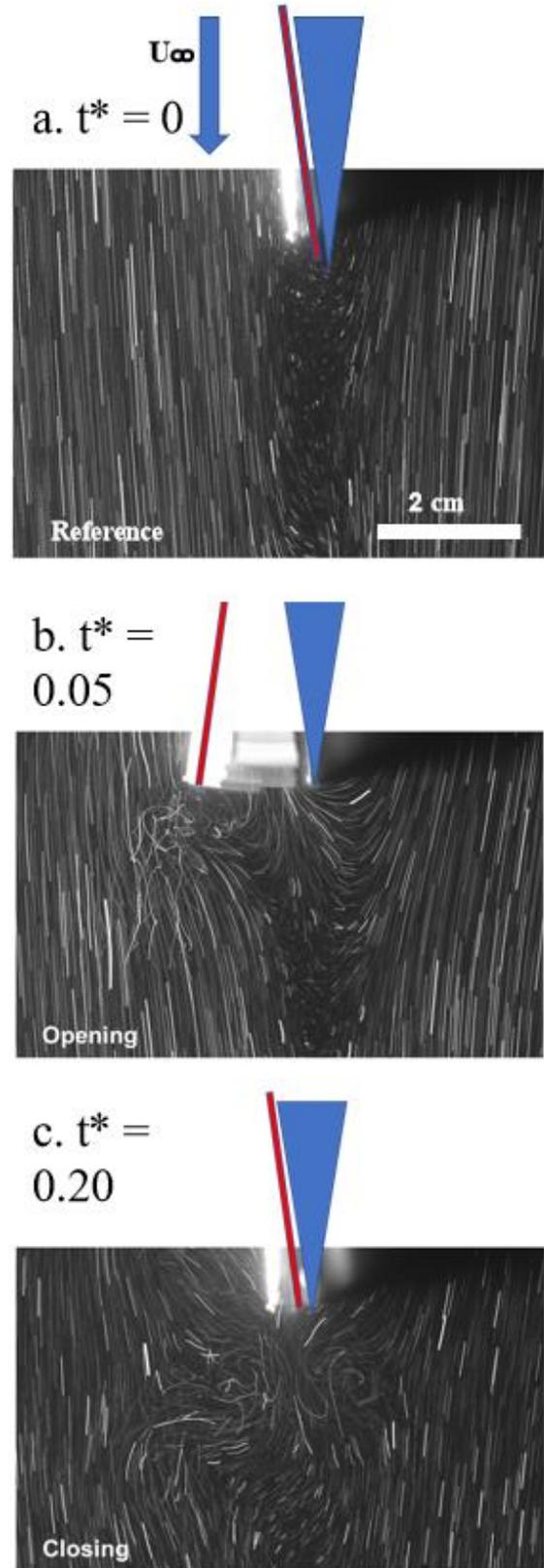
6

Figure 9: Flow visualisation using multi-exposed particle traces during reference (a), opening (b), and closing (c) of the trailing edge flaplet row.
Source: This is an original figure produced by the authors.

a. Post actuation t*=0.2
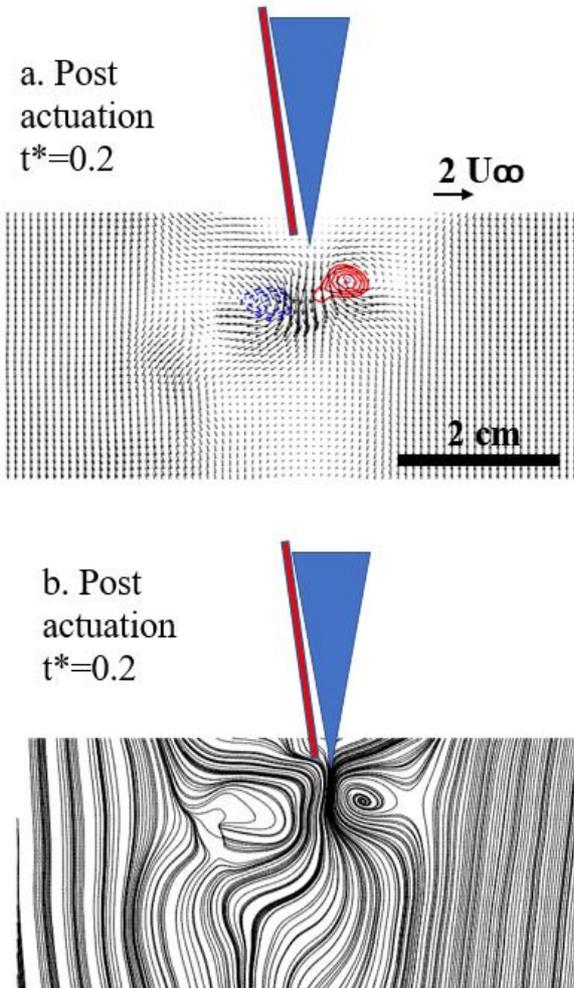
2 U∞

2 cm

b. Post actuation t*=0.2

Figure 10: Snapshot from the TR-PIV results after flaplet deployment showing: top – the starting vortices resulting from the flaplet deflection can be seen in the vector plot, and bottom – the radial entrainment of the trailing edge flow is further emphasised by observing the streamline plot. Red indicates anticlockwise and blue clockwise rotation.
Source: This is an original figure produced by the authors.

4.2 Lift condition

Another set of measurements were taken with the model at 5˚ angle of attack, to investigate a lift condition. The specific angle of attack was chosen, as it is at high lift to drag ratio, found by carrying out an XFLR5 (Drela, M., 1989). analysis on the aerofoil at Re=15000.

a. Pre-actuation
t*=0

1.5cm

b. Opening
t*=0.05
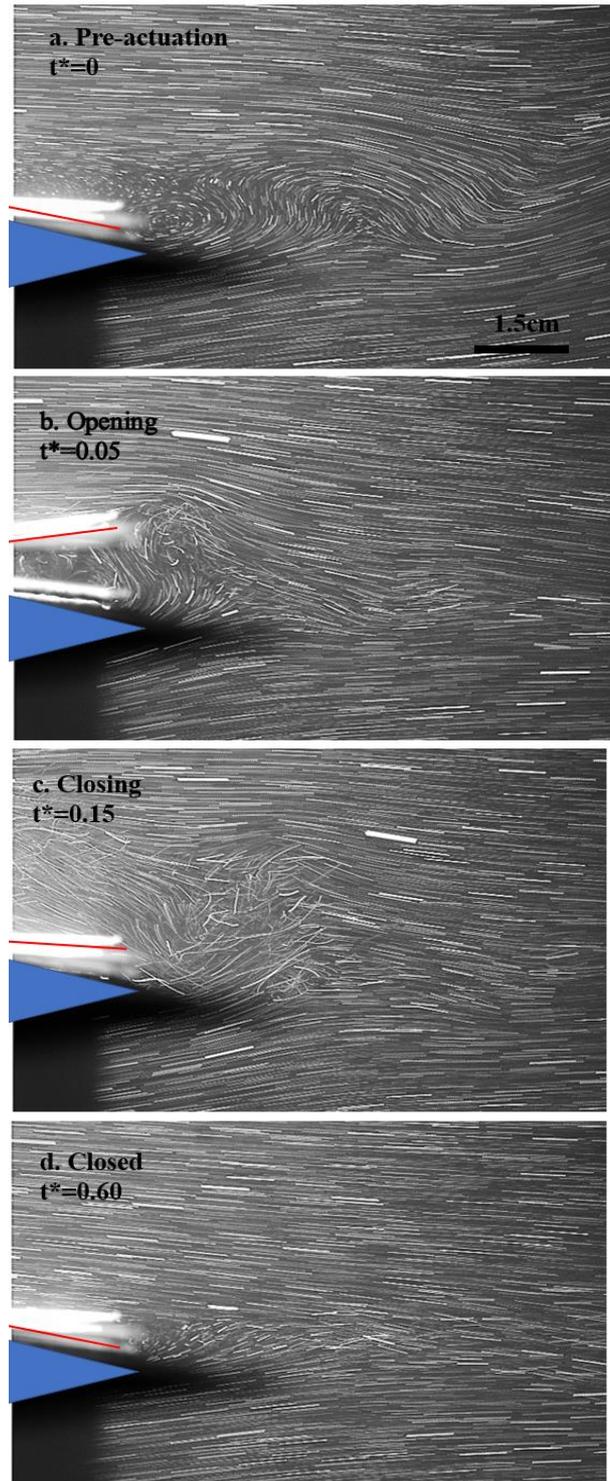
c. Closing
t*=0.15

d. Closed
t*=0.60

Figure 11: Flow visualisation in lift condition of the flow near the trailing edge (flow from left to right), using multi-exposed particle traces in four stages over one convection time. (a) trailing edge wake before start of actuation, (b) during deployment phase (opening), (c) immediately at the end of stowing phase, and (d) after one convective time from deployment start.

7

The flow visualisations in Fig.11 allowed for an improved understanding of the flow physics during and subsequently after the flaplet actuation. The control cycle captures part of the fluid from the wake during flaplet opening and then reenergises said fluid during the closure mechanism, by interrupting the wake at the trailing edge with strong streamwise momentum. What is particularly noticeable, is the introduction of a radial velocity component evident in Fig. 11b and Fig. 11 c immediately after the closing phase. This, coupled with the presence of a starting vortex, as seen in Fig. 10a, encourages the entrainment of the flow. The current principle induces the momentum due to the squeezing effect, similar to that shown in (Hess, et al., 2013) while the suction process entrains only fluid of low momentum from the near wake.
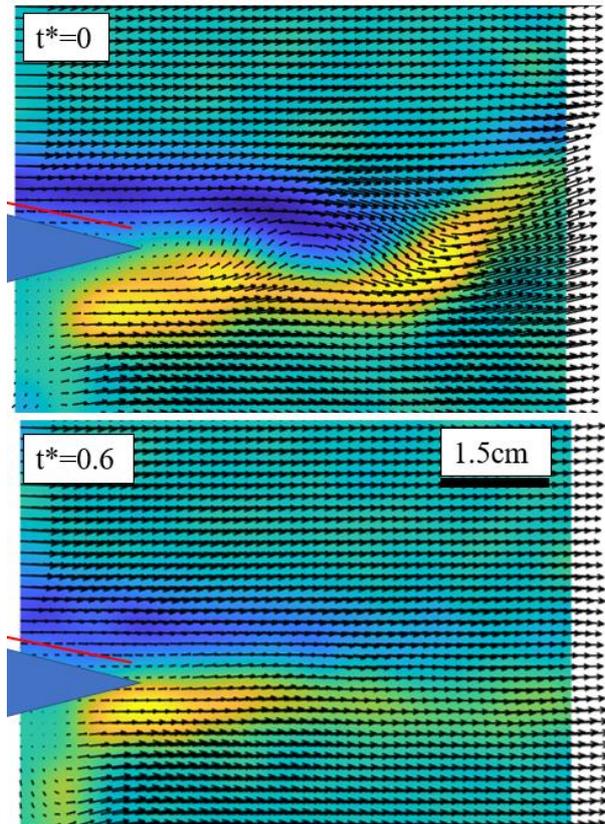

Figure 12: Velocity vectors overlaid on the colour coded vorticity field for two time instances. During lift conditions. Conditions as in Fig. 11.

Fig. 12, above, shows the wake pattern corresponding to processed images form Fig 11 as a vector plot for t*=0 and t*=0.6. There is a noticeable increase in streamwise velocity in the near-wake after the flaplet actuation. The vorticity field shows a transformation of the typical undulating wake pattern into a rather streamwise oriented straight flow with reduced peak values of vorticity at both sides of the wake. Additionally, the transversal, cross-wise flow component in the wake is seen to be reduced. , The effect post flaplet closure can be seen to persist for nearly one convective time after closure which is when the wake undulation resumes.
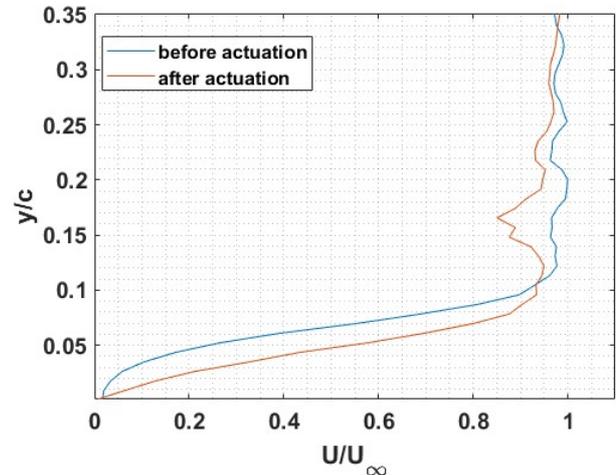

Figure 13: Instantaneous boundary layer profile at 0.95x/C, taken from the TR-PIV results used in Fig. 12 before and after the complete duty cycle of the flaplet (t*=0, t*=0.6). The reduction in boundary layer thickness is shown as a consequence of the actuation.

The entrainment effect after actuating the flaplets can be seen by observing the boundary layer profile before and after actuation, see Fig. 13. Before actuation, a typical boundary layer profile for a 5° AoA at Re = 15 000 can be seen with $\delta*$ of approximately 0.12. The profile shows the typical retardation near the wall in an adverse pressure gradient situation with the inflection point located away from the wall. After actuation, the entrainment effect has accelerated the near-wall flow and the profile is steeper.
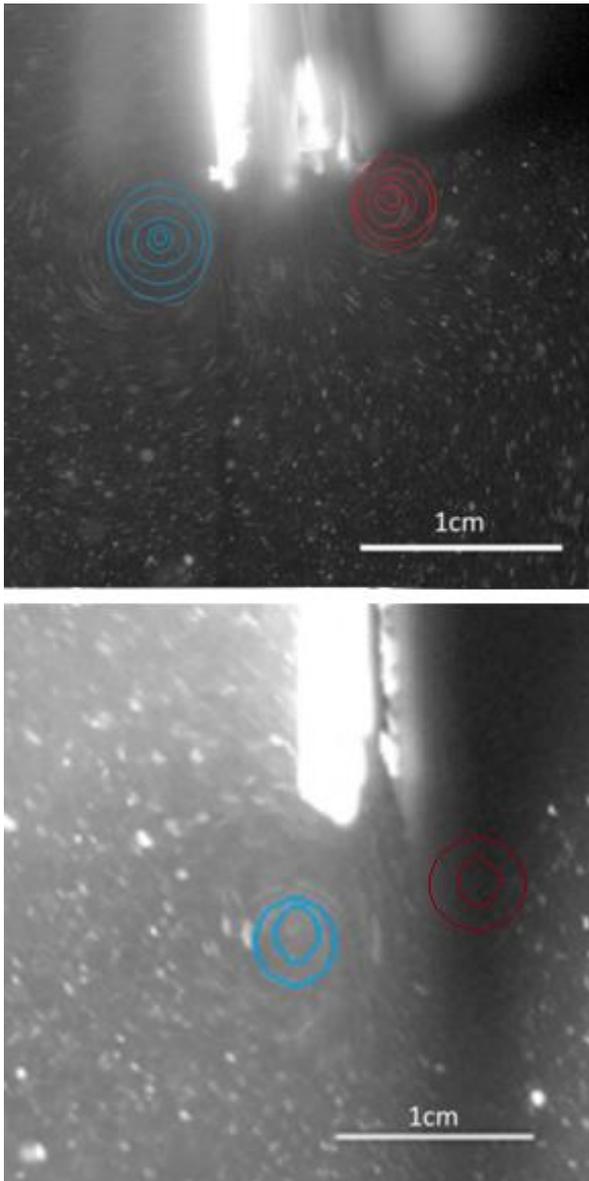
Figure 14: Close-up view on the formation of a pair of counter-rotating vortices generated by the flap closing motion. Top: situation with flap actuation with 4 adjoined flaplets compared to bottom with only one single flap actuated. The pressure side is within the PIV shadow for the bottom image.
Source: This is an original figure produced by the authors.

Furthermore, the deployment effect is reduced as the number of flaplets are reduced. Fig. 14 shows the comparison of the effect of a single flaplet deployment to multiple flaplets. It is observed that the starting vortices are smaller in size and are less coherent for a single flaplet than the clear pair of counter rotating vortices produced by the multiple adjoined flaplets. As expected, the added streamwise momentum due to flaplet closing effect is smaller for a single flaplet, and so are the

associated entrainment and wake reduction effects. As a consequence, the jet effect dissipates quicker for a single flap as compared to 4 adjoined flaps.

5. SUMMARY AND CONCLUSIONS OF INITIAL FINDINGS

The design of the flaplets for pneumatic actuation was illustrated and demonstrated as well as the pneumatic actuation within the experimental facility, using a high pressure air source. The design using flexible inflatable structures was outlined to provide a better understanding of the duty cycle internally (i.e. embedded within the aerofoil) and externally over the suction side of a NACA 0012 aerofoil. Such a pneumatic system could be applied to unmanned aerial systems by exploiting bleed air from gas turbine and micro-gas turbine engines in powered aircraft, or from onboard high pressure air sources as the system is completely closed loop.

Furthermore, the flow physics were studied for a given flap actuation cycle for single flaps and rows of adjacent flaps through a series of flow visualisations and TR-PIV experiments. The initial results presented herein show the feasibility of the pneumatic actuation principle of segmented flaps at the trailing edge for flow control. The action of the flaplets observed is to capture low momentum fluid from the near-wake region of the trailing edge during the opening phase, driven by the local suction in the increasing void between the flaplet and the surface. The closure phase then expels this fluid in form of a tangential jet, which re-energises via entrainment the fluid near the trailing edge and adds streamwise momentum to the wake. With the jet comes a pair of counter rotating vortices that propagate in the streamwise direction. The size and energy of the structure was shown to vary with the number of flaplets deployed. This mechanism is similar to the observation of jet formation on snapping shrimps, see Hess et al. (2013). In lifting conditions, the entrainment effect shows the reduction of the boundary layer thickness, which persists for at least one full convective time. This was illustrated by analysing the streamline and vector plots of the TR-PIV results and shown in flow visualisation images.

Further investigations will focus on the effect of increasing angle of attack of the aerofoil and local interaction of the flaplet with the outer flow near the trailing edge, especially for the purpose of active gust control. In addition, the flaplets may help to interrupt the

growth of separation bubbles on the aft part of the aerofoil by preventing upstream transport and re-.

6.   LIMITATIONS AND IMPROVEMENTS

The experiments of the model and the pneumatic actuation show that it can be used as a gust controller, however there are future improvements to be made. Currently improvements to the mechanical actuation are required, such that the duty cycle of the flaplets can be unconstrained and repeatable. This could be in the form of small integrated air sacks, such as the ones used as pneumatic lifting devices, as opposed to balloons. These sacks would be more suited to cyclic opening and closing, as well as prolonged periods of inflation. Another improvement would be to use spark erosion to remake the metal flaplets, removing manufacturing discrepancies and ensuring that every flaplet is identical. Spark erosion would also help to improve the hinge mechanism, reducing inconsistencies in flaplet opening.

7.   OUTLOOK

The concept using the flaplet actuators shows promise for beneficial gust control based on the observed flow manipulation near the trailing edge, (suction of low momentum fluid from the trailing edge near-wake and successive tangential blowing into the wake). The capability that the flaplets have shown to reduce the momentum thickness within the wake, as represented by the boundary layer thickness change found in this paper has implications on instantaneous drag. Due to the short duty cycle relative to the convective time shown, the application has potential to be used as a method of reaction to instabilities due to short term gusts on small and medium sized unmanned aerial systems.

The deflection of the flaplets can be compared to deploying a simple hinged flaplet of various aspect ratios. Thus, the rise and discontinuity in pressure resulting from such a deflection will form tip vortices that vary with the aspect ratio (or number) of flaplets deployed. This paper has shown that the size and energy of the starting vortices varies with the number of flaplets deployed. Further work will explore the interaction between the tip vortices generated by simultaneous deployment of flaplets separated in the spanwise direction in more complicated spanwise patterns. Further studies are planned on the gust controller to test for higher angles of attack and the modification of the flow by the flaplet action in such circumstances. In addition, different patterns of duty cycles (opening time – fully open -closing time) will be investigated to find the optimum parameter for different control aspects, such as prevention of separation growth, or interruption of the wake relative to the characteristic timescales of these flow formation features.

8.   ACKNOWLEDGEMENTS

9. REFERENCES

Brücker, C., Schlegel, D. & Triep, M., 2016. Feather vibration as a stimulus for sensing incipient separation in falcon diving flight.. Natural Responses, 7(7), pp. 411-422.

Chanzy, Q. & Keane, A., 2018. Analysis and experimental validation of morphing UAV wings.. The Aeronautical Journal, 122(1249), pp. 390-408.

Court, A., 2021. Trailing Edge Pneumatic Systems for Flow Control (master thesis). London: City, University of London.

Drela, M., 1989. XFOIL: An analysis and design system for low Reynolds number airfoils. In Low Reynolds Number Aerodynamics: Proceedings of the Conference Notre Dame, Indiana, USA, 5–7 June 1989 (pp. 1-12). Springer Berlin Heidelberg.

Hess, D., Bruecker, C. & Hegner, F., 2013. Vortex formation with a snapping shrimp claw. PloS ONE, 8(11), pp. 1-10.

Mohamed, A., Watkins, S., Clothier, R., Abdulrahim, M., Massey, K. and Sabatini, R., 2014. Fixed-wing MAV attitude stability in atmospheric turbulence—Part 2: Investigating biologically-inspired sensors. Progress in Aerospace Sciences, 71, pp.1-13.

Pankonien, A. M., & Inman, D. J. (2014). Aerodynamic performance of a spanwise morphing trailing edge concept. In 25th International Conference on Adaptive Structures and Technologies.

Selim, O. et al., 2021. The Peregrine Falcon's Dive: On the Pull-Out Manoeuvre and Flight Control Through Wing-Morphing.. AIAA, 59(10), pp. 3979-3987.

Siefert, E., Reyssat, E., Bico, J. & Roman, B., 2019. Bio-inspired pneumatic shape morphing elastomers.. Nature Material, 18(1), pp. 24-28.

Talboys, E., Geyer, T. F., & Brücker, C. (2019). An aeroacoustic investigation into the effect of self-oscillating trailing edge flaplets. Journal of Fluids and Structures, 91, 102598.

Worcester, S.E, 1996. The scaling of the size and stiffness of primary flight feathers. Journal of zoology, 239(3), pp.609-624